Photoionization and electron-impact ionization of Ar^{5+}

Jing Cheng Wang, M. Lu, D. Esteves, M. Habibi, G. Alna'washi, and R. A. Phaneuf

Department of Physics, MS 220, University of Nevada, Reno, Nevada 89557-0058, USA

A. L. D. Kilcoyne

Advanced Light Source, LBNL, MS 7-100, Berkeley, California 94720-8225, USA

(Received 27 February 2007; published 27 June 2007)

Absolute cross sections for photoionization and electron-impact ionization of Ar^{5+} have been measured using two different interacting-beams setups. The spectra consist of measurements of the yield of products due to single ionization as a function of electron or photon energy. In addition, absolute photoionization and electron-impact ionization cross sections were measured to normalize the measured Ar^{6+} product-ion yield spectra. In the energy range from 90 to 111 eV, both electron-impact ionization and photoionization of Ar^{5+} are dominated by indirect 3s subshell excitation-autoionization. In the energy range from 270 to 285 eV, resonances due to 2p-3d excitation-autoionization are prominent in the photoionization spectrum. In the range from 225 to 335 eV, an enhancement due to 2p-nl ($n > 2$) excitations are evident in the electron-impact ionization cross section. The electron and photon impact data show some features due to excitation of the same intermediate autoionizing states.

I. INTRODUCTION

The properties of multiply ionized, excited atoms are of both fundamental and practical interest. Excited ions play important roles in the diagnostics of laboratory and astrophysical plasmas. Noble gases are important in controlled fusion experiments, where they are introduced as diagnostic impurities to probe the central core. With only one 3p electron outside of filled subshells, Ar^{5+} is a multiply charged ion with a relatively simple atomic structure, and can provide detailed information about core-electron excitations in both photoionization and electron-impact ionization of a many-body electronic system.

The ground-state term of Ar^{5+} is $(1s^2 2s^2 2p^6 3s^2 3p)$ $^2P_{1/2}$, and the $^2P_{3/2}$ metastable state shares the same configuration. The NIST atomic spectra database [1] gives the ground-state ionization potential as 91.0 eV and the $^2P_{1/2}$-$^2P_{3/2}$ fine-structure splitting as 0.274 eV. Ionization of Ar^{5+} has been studied previously by both photon [2] and electron impact [3,4]. However, the published electron-impact experiments obtained only absolute values of the cross section at discrete energy points, whereas the aim of the present study was to uncover finer spectroscopic details. The only published Ar^{5+} photoionization study focused on calculations for the Opacity Project [5].

II. EXPERIMENTAL TECHNIQUES

The experimental data were obtained using two different interacting-beams experimental setups. The apparatus for studying electron-impact ionization of ions is part of the Multicharged-Ion Research Facility in the Physics Department at University of Nevada, Reno [6,7]. The photoionization studies were performed using the ion-photon beam (IPB) endstation [8,9] installed on beamline 10.0.1.2 at the Advanced Light Source (ALS). Since details of the experimental setups and measurement techniques have been reported, only a brief description is presented here.

A. Photoionization experiment

The ^{40}Ar^{5+} ions for the photoionization experiment were produced by a compact 10 GHz all-permanent-magnet electron cyclotron resonance (ECR) ion source, and extracted using a 6 kV positive potential. After extraction, the ion beam was focused by a cylindrical einzel lens and ^{40}Ar^{5+} ions were separated from other charge states by a 60° analyzing magnet according to the momentum-to-charge ratio. The Ar^{5+} ion beam was further focused, steered, and positioned by a second set of electrostatic elements and directed to a spherical electrostatic deflector that merged it onto the axis of a beam of synchrotron radiation. The latter was generated by an undulator and monochromatized by a spherical-grating monochromator. The Ar^{6+} photoion yield was measured as a function of photon energy in the range of 90–111 eV and 270–285 eV. The photon energy scale was calibrated to within ±0.01 eV by measuring accurately known resonances using a gas cell containing Kr, Ar or CO_2 [10,11].

To determine cross sections, two-dimensional spatial profiles of the merged ion and photon beams were measured by three translating-slit scanners installed in a central interaction region of length 29.4-cm. A 45° demerging magnet separated the Ar^{6+} products from the primary beam which was collected in a Faraday cup. The Ar^{6+} product ions were further directed by a spherical electrostatic deflector to a single-particle detector and counted. Absolute photoionization cross sections were measured at several discrete photon energies to normalize the photoion-yield spectrum. A potential of 1.2 kV was applied to the interaction region to energy-label Ar^{6+} product ions produced therein. The photon beam was mechanically chopped to subtract background produced by collisions of Ar^{5+} with residual gas. The total uncertainty of the photoionization cross-section measurements is estimated to be ±17%.

B. Electron-impact ionization experiment

The electron-impact ionization experiment is conceptually similar to the photoionization experiment, but uses crossed
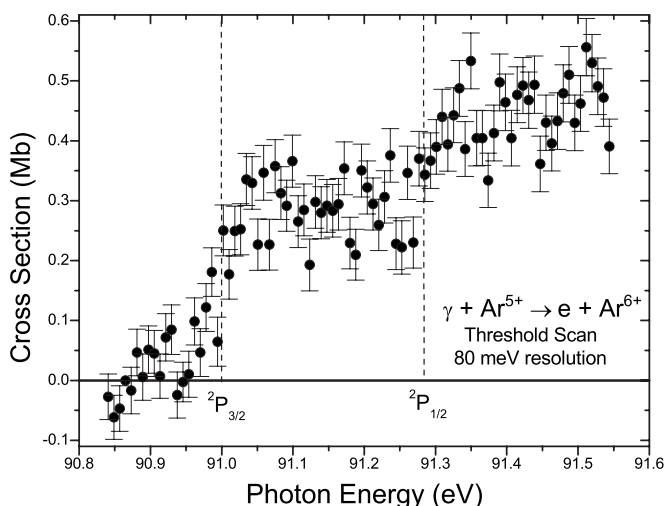
FIG. 1. Photoionization cross-section measurement in the threshold energy region at a spectral resolution of 80 meV. The dashed lines indicate the thresholds of the $^2P_{1/2}$ ground state and the $^2P_{3/2}$ metastable state determined from these measurements.

rather than merged beams. The $^{40}\text{Ar}^{5+}$ ions were produced by a 14.4 GHz ECR ion source and extracted via a 10 kV positive potential. After extraction, the ion beam was focused and steered by sets of einzel lenses and steering plates, and $^{40}\text{Ar}^{5+}$ was separated from other charge states by a 90° analyzing magnet. After deflection by a 90° electrostatic analyzer, the Ar^{5+} beam intersected a monoenergetic electron beam at right angles. The Ar^{6+} products were separated from the primary beam by a 90° analyzing magnet. After further deflection by a 90° electrostatic analyzer, the product ions were counted by a single-particle detector. The Ar^{5+} primary ions were collected in a Faraday cup mounted inside the analyzing magnet chamber. The electron gun could be translated mechanically across the ion beam, allowing measurement of the electron-impact ionization cross section by the animated-beams technique [12–14]. Cross sections were measured at several discrete electron energies to normalize the Ar^{6+} product-ion-yield spectrum which was recorded in 0.07 eV energy steps. The spectrum was obtained by repeating the energy scans as many as 100 times to obtain high statistical precision. The total uncertainty of the electron-impact ionization cross-section measurement in this experiment is estimated to be ±11%.

III. EXPERIMENTAL RESULTS AND ANALYSIS

A. Photoionization of Ar^{5+}

1. Near-threshold region

Measurements of the cross section for single photoionization of Ar^{5+} in the near-threshold region taken with a photon energy resolution of 0.08 eV are shown in Fig. 1. This measurement was performed to determine the ionization potential with high precision and to estimate the fraction of metastable Ar^{5+} in the primary ion beam. The measured ionization potentials of the ground state $[3s^2 3p]$ $^2P_{1/2}$ and metastable state $[3s^2 3p]$ $^2P_{3/2}$ are 91.29±0.01 eV, and

91.00±0.01 eV, respectively. The tabulated ionization potential of the ground state in the NIST database is 91.0 eV, which is 0.29 eV below the experimental result. From the experiment, the energy difference between the ground and metastable states, which is the fine structure splitting, is 0.290±0.014 eV, which compares favorably with the value of 0.274 eV tabulated in the NIST database.

Since the $^2P_{1/2}$-$^2P_{3/2}$ fine-structure energy splitting is small compared to the ionization potential, a relative population in the ion beam based on their statistical weights ($2J+1$) is expected. The measured ratio of the heights of the two steps in Fig. 1 is 1.8, which is close to the statistical prediction of 4/2. The present measurements are therefore considered to correspond to a sum of the ground-state cross section multiplied by 1/3 and the metastable-state cross section multiplied by 2/3. Three additional metastable states, $[3s3p^2]$ $^4P_{1/2,3/2,5/2}$, lie about 12 eV above the ground state with lifetimes in the microsecond range [15]. Since the measured photoionization cross section below the $[3s^2 3p]$ $^2P_{3/2}$ metastable state is consistent with zero, these states do not appear to be appreciably populated in the primary ion beam.

2. 2p→3d excitation-autoionization

Panel (a) of Fig. 2 shows absolute measurements in the range of 273 to 284 eV taken at a resolution of 0.08 eV. Open circles with error bars indicate individual absolute cross-section measurements, to which the relative scan was normalized. The resonances in this energy range are attributed to 2p-3d inner-shell excitations followed by autoionization. The total experimental oscillator strength determined by integrating the cross section in this energy range [16] is 1.99. The oscillator strength due to 2p-3d transitions was calculated using the Cowan atomic structure code [17], taking into account the statistical admixture of the ground state and the metastable state in the primary ion beam. This predicts a total oscillator strength of 1.75, within 12% of the measurement and well within the ±17% experimental uncertainty. To compare with the experimental result, a theoretical spectrum was synthesized from the calculated oscillator strengths for transitions in this energy range and convoluted with a Gaussian profile [0.08 eV full width at half maximum (FWHM)] to account for the instrumental function. The theoretical spectrum shown in panel (b) of Fig. 2 agrees reasonably well with the experimental results.

3. 3s→np (n>5) excitation-autoionization

Panel (a) of Fig. 3 shows absolute photoionization measurements in the energy range from 90 to 111 eV at a photon-energy resolution of 0.08 eV. Resonances in this energy range are attributed to 3s-np (n>5) inner-shell excitations. Again, a synthetic spectrum was calculated using the Cowan atomic structure code and convoluted with a Gaussian profile of 0.08 eV FWHM shown in panel (b) of Fig. 3, in which the calculated spectrum was arbitrarily shifted by +1.23 eV to more closely match the energy scale of the measurements. In order to determine the oscillator strength for 3s-np (n>5) transitions from the measurements, the nonzero direct photoionization cross section was first subtracted from the experimental results.
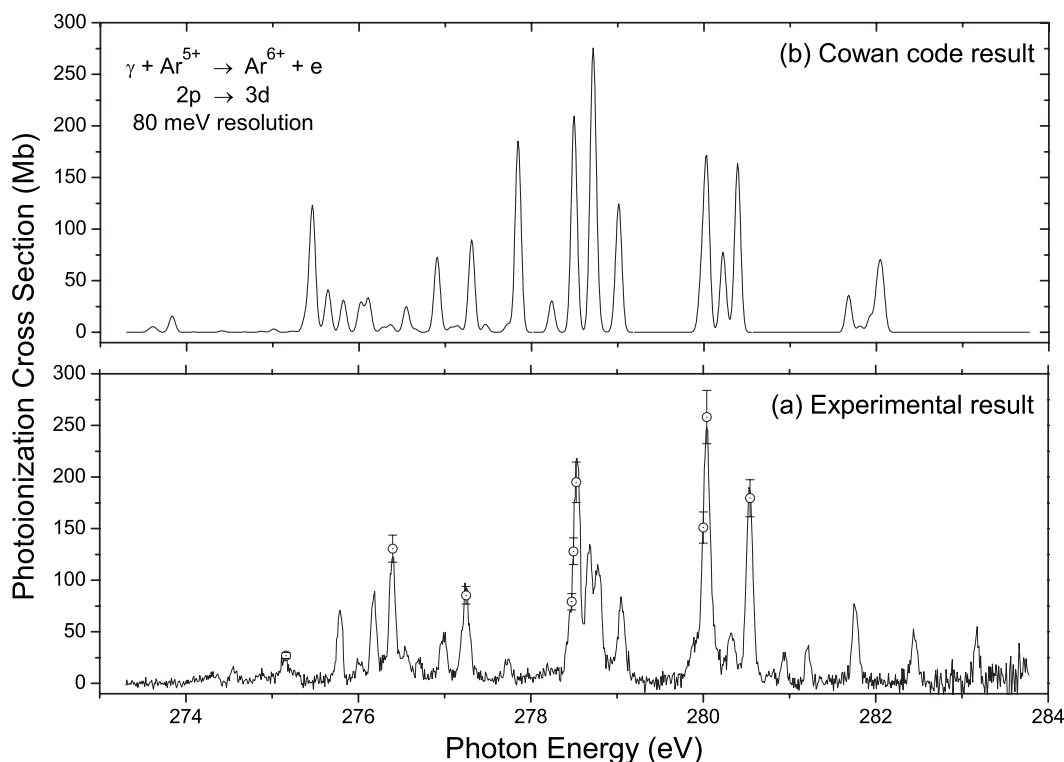
FIG. 2. Comparison of cross-section measurements for photoionization of Ar^{5+} in the energy range of 273–284 eV taken at a resolution of 80 meV with a resonance spectrum calculated using the Cowan atomic structure code. The calculation was convoluted with a Gaussian profile of 80 meV FWHM. The open circles with error bars are absolute measurements.

Three Rydberg series are identified in this energy range. As shown in panel (a) of Fig. 3, square symbols denote unresolved transitions (series 1) due to $3s^23p^1$ $(^2P_{3/2})$-$3s^13p^1$ (^3P) np^1 $(^2D_{5/2})$ $(n>6)$ (transition 1) and $3s^23p^1$ $(^2P_{1/2})$-$3s^13p^1$ (^3P) np^1 $(^2D_{3/2})$ $(n>6)$ (transition 2), up-triangle symbols denote the transitions (series 2) due to $3s^23p^1$ $(^2P_{3/2})$-$3s^13p^1$ (^1P) np^1 $(^2D_{5/2})$ $(n>5)$, and down-triangle symbols denote the transitions (series 3) due to $3s^23p^1$ $(^2P_{1/2})$-$3s^13p^1$ (^1P) np^1 $(^2D_{3/2})$ $(n>5)$. Spectroscopic assignments of the individual resonances identified in Fig. 3 are given in Table I and II present a comparison between calculated and experimental results of the series limits and quantum defects of these identified series.

In this case, the total f value from experiment corresponds to the total integrated oscillator strength for the spectrum shown in Fig. 3. The total calculated f value represents the sum of all $3s$-np $(5<n<14)$ autoionizing transitions in this energy range. The difference between experimental result and the calculation is 8.4%. Considering the absolute experimental uncertainty of ±17% and the fact that the oscillator strengths of the various series for $n>13$ are not included, the level of agreement with the calculation is considered satisfactory.

Figure 4 presents a measurement of the first resonance feature, labeled 1 in panel (a) of Fig. 3 at a higher photon energy resolution of 0.02 eV, showing it to be a combination of at least nine resonances. The corresponding spectrum calculated using the Cowan atomic structure code and convoluted with a Gaussian profile of 0.02 eV FWHM is again brought into reasonable agreement with the measurement by

shifting the calculated spectrum by +1.23 eV. Table III gives detailed information about the identified features presented in Fig. 4.

Again, the total f values from calculation and experiment indicate the total oscillator strength due to the transitions in this energy region, and not the sum of the tabulated f values. Here, the calculated total oscillator strength is 17% lower than the measured result, still within the experimental uncertainty. Features 1a and 1e are due to the transitions from the metastable state $(^2P_{3/2})$ and the ground state $(^2P_{1/2})$, respectively, to the same final state $(^2P_{3/2})$. The energy difference between features 1a and 1e of 0.282±0.011 eV corresponds to the fine-structure splitting. This value is consistent with the fine structure splitting measurement determined from the observed $^2P_{1/2}$ and $^2P_{3/2}$ ionization thresholds of 0.290±0.014 eV.

B. Electron-impact ionization of Ar^{5+}

Measured cross sections for electron-impact single-ionization of Ar^{5+} in the energy range 53–335 eV are shown in Fig. 5. The relative yield of Ar^{6+} product ions was measured in a fine energy-scanning mode and normalized to absolute cross-section measurements made during the current experiment. The electron energy resolution is approximately 1 eV. For comparison, also shown in Fig. 5 are the experimental results of Zhang et al. [3], Gregory and Crandall [18], and the single-parameter Lotz formula for direct single ionization of Ar^{5+}.

The ionization onset from the electron-impact ionization measurement is determined to be 89.8±1.9 eV, indicating
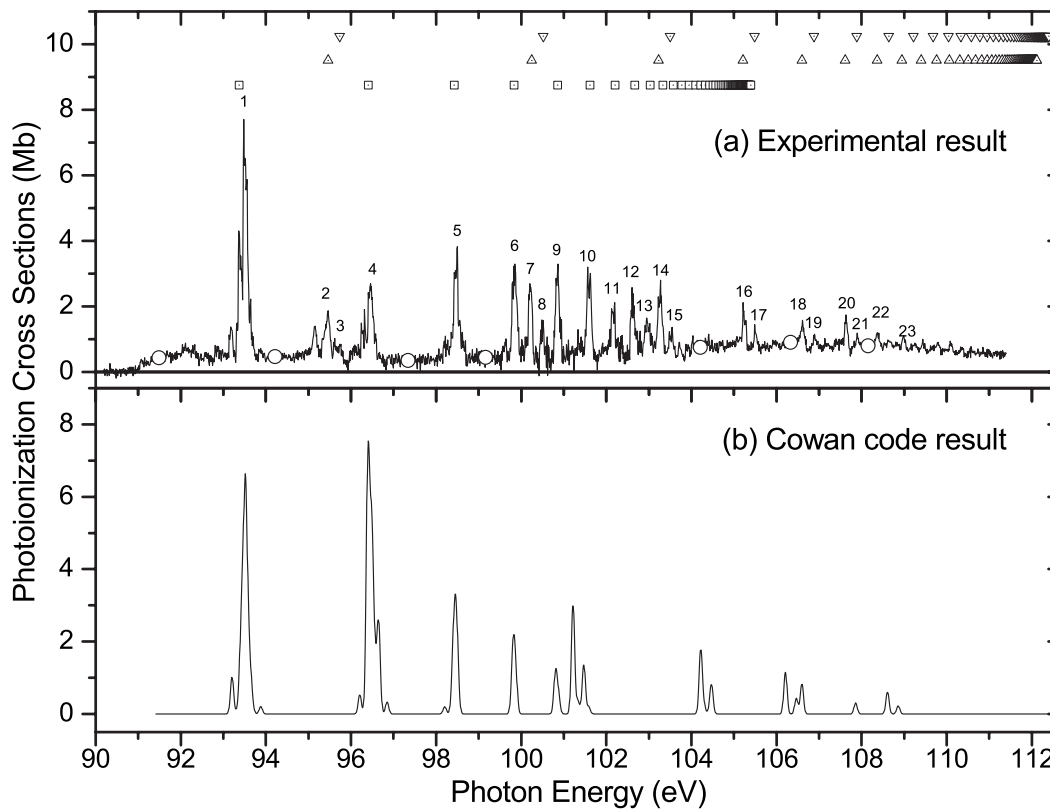
FIG. 3. Comparison of absolute cross-section measurements for photoionization of Ar^{5+} with the calculated spectrum in energy range of 90–111 eV. The energy scale of the calculated spectrum has been shifted by +1.23 eV in this case to better match the experiment. Open circles are absolute measurements.

that the parent Ar^{5+} ion beam contained ions in the $[3s^23p]$ $^2P_{3/2}$ metastable state. This is consistent with the photoionization measurement, in which the ionization potentials of the ground state $[3s^23p]$ $^2P_{1/2}$ and the metastable state $[3s^23p]$ $^2P_{3/2}$ were determined to be 91.29 ± 0.01 eV, and 91.00 ± 0.01 eV, respectively. As in the photoionization measurements, the ionization onset in the current electron-impact ionization data shows no evidence of metastable states due to the configuration $3s3p^2$, as observed by Zhang *et al.* [3]. Further evidence is that the resonant excitation-double-autoionization (REDA) feature from the $3s3p^2$ configuration near 130 eV described by Zhang *et al.* [3] was not observed in the current experiment. The present measurements from the ionization threshold to 130 eV are in good agreement with the experimental results of Gregory and Crandall [18], which also show no evidence of $3s3p^2$ metastables.

The electron-impact ionization cross section rises more steeply from the ionization threshold than the Lotz formula prediction for direct ionization. This suggests contributions to the cross section due to excitation-autoionization. A series of onsets due to $3s$-nl ($n > 5$) transitions is likely responsible for most of the enhancement of the cross section over direct ionization in this energy range. It is noted that $3s$-np ($n > 6$) transitions contribute to the measured photoionization cross section in this photon energy range. Whether the enhancement of the electron-impact ionization cross section in this energy range is due to $3s$-np ($n > 6$) transitions or electric-dipole-forbidden transitions (e.g. $3s$-ns, $3s$-nd) can-

not be determined from the current experiment.

Figure 6 shows the measured electron-impact ionization cross section for Ar^{5+} in the energy range from 225 to 335 eV. The configuration-average excitation and ionization energies of $2p$-nl transitions, together with the lowest energy levels of each transition, are marked by the short vertical lines in Fig. 6. There is some correspondence between the predicted energies and the measured features. A change of slope beginning near 270 eV suggests that it is due to $2p$-$3d$ transitions, which were observed to be strong in the photoionization experiment. The largest feature in this energy range is an apparent step in the electron-impact ionization cross section near 241 eV, where $2p$-$3p$ transitions are predicted to occur. Such transitions are forbidden in photoionization, but appear to be responsible for the largest features in the electron-impact ionization cross section starting near 241 eV.

An apparent resonance feature observed near 250 eV, which is below the excitation threshold for $2p$-$3d$ transitions, is attributed to REDA involving the $2p^53s^23p^2nl$ intermediate autoionizing states of Ar^{4+} that decay by sequential ejection of two electrons. A possible reaction pathway is as follows:

$$\begin{aligned} Ar^{5+}(2p^63s^23p) + e &\rightarrow Ar^{4+}(2p^53s^23p^2nl) \\ &\rightarrow Ar^{5+}(2p^63s3p^2) + e^- \\ &\rightarrow Ar^{6+}(2p^63s^2) + 2e^-. \end{aligned}$$

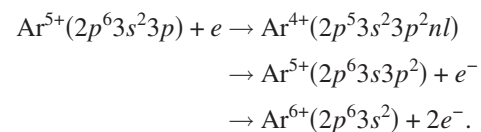TABLE I. Spectroscopic assignments of the features identified in Fig. 3. The uncertainties in the energy measurements are ±0.01 eV. Oscillator strengths calculated using the Cowan atomic structure code are weighted by the estimated initial-state populations in the experiment (2/3 for $^2P_{3/2}$ and 1/3 for $^2P_{1/2}$) and presented as "(CAL)." The oscillator strengths determined from experiment are presented as "(EX)."

Feature	Energy (eV)	Quantum defect δ	Series limit (eV)	Assignment	Weighted f value (CAL)	f value (EX)
1	93.48	0.62	105.42	$3s^23p^1(^2P_{3/2})$-$3s^13p^1(^3P)7p^1$ $(^2D_{5/2})$	0.0038	0.0041
				$3s^23p^1(^2P_{1/2})$-$3s^13p^1(^3P)7p^1$ $^2D_{3/2}$	0.0017	0.0041
2	95.46	0.58	112.14	$3s^23p^1(^2P_{3/2})$-$3s^13p^1(^1P)6p^1$ $(^2D_{5/2})$	0.0026	0.0021
3	95.74	0.58	112.41	$3s^23p^1(^2P_{1/2})$-$3s^13p^1(^1P)6p^1$ $(^2D_{3/2})$	0.0016	0.0009
4	96.48	0.62	105.42	$3s^23p^1(^2P_{3/2})$-$3s^13p^1(^3P)8p^1$ $(^2D_{5/2})$	0.0023	0.0039
				$3s^23p^1(^2P_{1/2})$-$3s^13p^1(^3P)8p^1$ $(^2D_{3/2})$	0.0012	
5	98.50	0.62	105.42	$3s^23p^1(^2P_{3/2})$-$3s^13p^1(^3P)9p^1$ $(^2D_{5/2})$	0.0015	0.0029
				$3s^23p^1(^2P_{1/2})$-$3s^13p^1(^3P)9p^1$ $(^2D_{3/2})$	0.0008	
6	99.83	0.62	105.42	$3s^23p^1(^2P_{3/2})$-$3s^13p^1(^3P)10p^1$ $(^2D_{5/2})$	0.0011	0.0028
				$3s^23p^1(^2P_{1/2})$-$3s^13p^1(^3P)10p^1$ $(^2D_{3/2})$	0.0006	
7	100.21	0.58	112.14	$3s^23p^1(^2P_{3/2})$-$3s^13p^1(^1P)7p^1$ $(^2D_{5/2})$	0.0015	0.0018
8	100.51	0.58	112.41	$3s^23p^1(^2P_{1/2})$-$3s^13p^1(^1P)7p^1$ $(^2D_{3/2})$	0.0009	0.0006
9	100.86	0.62	105.42	$3s^23p^1(^2P_{3/2})$-$3s^13p^1(^3P)11p^1$ $(^2D_{5/2})$	0.0007	0.0019
				$3s^23p^1(^2P_{1/2})$-$3s^13p^1(^3P)11p^1$ $(^2D_{3/2})$	0.0004	
10	101.56	0.62	105.42	$3s^23p^1(^2P_{3/2})$-$3s^13p^1(^3P)12p^1$ $(^2D_{5/2})$	0.0006	0.0021
				$3s^23p^1(^2P_{1/2})$-$3s^13p^1(^3P)12p^1$ $(^2D_{3/2})$	0.0003	
11	102.20	0.62	105.42	$3s^23p^1(^2P_{3/2})$-$3s^13p^1(^3P)13p^1$ $(^2D_{5/2})$	0.0004	0.0011
				$3s^23p^1(^2P_{1/2})$-$3s^13p^1(^3P)13p^1$ $(^2D_{3/2})$	0.0002	
12	102.63	0.62	105.42	$3s^23p^1(^2P_{3/2})$-$3s^13p^1(^3P)14p^1$ $(^2D_{5/2})$	0.0003	0.0012
13	102.95	0.62	105.42	$3s^23p^1(^2P_{3/2})$-$3s^13p^1(^3P)15p^1$ $(^2D_{5/2})$	0.0003	0.0008
14	103.28	0.62	105.42	$3s^23p^1(^2P_{3/2})$-$3s^13p^1(^3P)16p^1$ $(^2D_{5/2})$	0.0002	0.0017
		0.58	112.14	$3s^23p^1(^2P_{3/2})$-$3s^13p^1(^1P)8p^1$ $(^2D_{5/2})$	0.0009	

TABLE I. (*Continued.*)

Feature	Energy (eV)	Quantum defect δ	Series limit (eV)	Assignment	Weighted f value (CAL)	f value (EX)
15	103.55	0.62	105.42	$3s^23p^1(^2P_{3/2})$-$3s^13p^1(^3P)17p^1$ $(^2D_{5/2})$	0.0002	0.0005
		0.58	112.41		0.0006	
				$3s^23p^1(^2P_{1/2})$-$3s^13p^1(^1P)8p^1$ $(^2D_{3/2})$		
16	105.22	0.58	112.14	$3s^23p^1(^2P_{3/2})$-$3s^13p^1(^1P)9p^1$ $(^2D_{5/2})$	0.0006	0.0007
17	105.49	0.58	112.41	$3s^23p^1(^2P_{1/2})$-$3s^13p^1(^1P)9p^1$ $(^2D_{3/2})$	0.0004	0.0002
18	106.61	0.58	112.14	$3s^23p^1(^2P_{3/2})$-$3s^13p^1(^1P)10p^1$ $(^2D_{5/2})$	0.0004	0.0004
19	106.89	0.58	112.41	$3s^23p^1(^2P_{1/2})$-$3s^13p^1(^1P)10p^1$ $(^2D_{3/2})$	0.0003	0.0001
20	107.63	0.58	112.14	$3s^23p^1(^2P_{3/2})$-$3s^13p^1(^1P)11p^1$ $(^2D_{5/2})$	0.0003	0.0005
21	107.89	0.58	112.41	$3s^23p^1(^2P_{1/2})$-$3s^13p^1(^1P)11p^1$ $(^2D_{3/2})$	0.0002	0.0001
22	108.41	0.58	112.14	$3s^23p^1(^2P_{3/2})$-$3s^13p^1(^1P)12p^1$ $(^2D_{5/2})$	0.0002	0.0003
23	108.98	0.58	112.14	$3s^23p^1(^2P_{3/2})$-$3s^13p^1(^1P)13p^1$ $(^2D_{5/2})$	0.0002	0.0002
Total					0.0452	0.0493

Variations on this scheme are possible. For example, in the second step the $3p$ electron may be ejected instead of the nl electron. In addition, the multiply excited intermediate state of Ar^{4+} could decay by autodouble ionization, i.e., the simultaneous emission of two Auger electrons. However, the resonant-excitation auto-double ionization (READI) process has a relatively low probability [19].

IV. SUMMARY AND CONCLUSIONS

Absolute cross sections were measured for photoionization of Ar^{5+} in the photon energy ranges from 90 to 111 eV and from 270 to 285 eV. The detailed energy dependence of the cross section for electron-impact ionization was also

TABLE II. Comparison between experimental results for the quantum defects and series limits of identified series and predictions using the Cowan atomic structure code.

	Quantum defect		Series limit (eV)	
	Experiment	Prediction	Experiment	Prediction
Series 1	0.62±0.01		105.42±0.01	
Transition 1		0.56±0.01		104.08±0.01
Transition 2		0.56±0.01		104.15±0.01
Series 2	0.59±0.01	0.58±0.01	111.90±0.01	112.14±0.01
Series 3	0.59±0.01	0.58±0.01	112.16±0.01	112.41±0.01

measured in the electron energy range from 53 to 335 eV. Both photoionization and electron-impact ionization of Ar^{5+} are dominated by indirect excitation-autoionization processes. Features are identified in both measurements that correspond to excitation of the same intermediate autoionizing configurations.
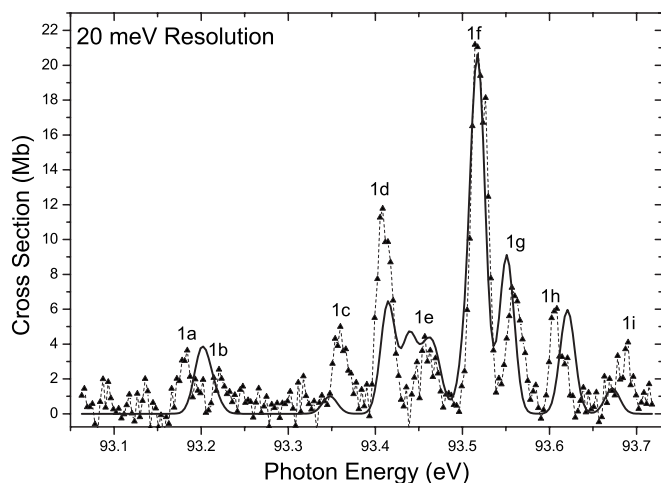

FIG. 4. Comparison between predicted and experimental results for the first resonance in Fig. 3. The dashed curve with triangle symbols is the experimental result, taken at a resolution of 20 meV. The solid curve is a calculation convoluted with a Gaussian profile, 20 meV FWHM, shifted by +1.23 eV.

TABLE III. Spectroscopic assignments of the features identified in Fig. 4. The uncertainties in the energy measurements are ±0.01 eV. Oscillator strengths calculated using the Cowan atomic structure code are weighted by the initial-state populations (see Table I) and presented as (CAL). The oscillator strengths determined from experiment are presented as (EX).

Feature	Energy (eV)	Assignment	Weighted f value (CAL)	f value (EX)
1a	93.18	$3s^2 3p^1(^2P_{3/2})$-$3s^1 3p^1(^3P)7p^1(^2P_{3/2})$	0.0005	0.0005
1b	93.22	$3s^2 3p^1(^2P_{3/2})$-$3s^1 3p^1(^1P)7p^1(^2P_{1/2})$	0.0001	0.0003
1c	93.36	$3s^2 3p^1(^2P_{1/2})$-$3s^1 3p^1(^1P)7p^1(^4D_{1/2})$	0.0002	0.0007
1d	93.41	$3s^2 3p^1(^2P_{3/2})$-$3s^1 3p^1(^3P)7p^1(^4P_{3/2})$	0.0012	0.0019
1e	93.46	$3s^2 3p^1(^2P_{1/2})$-$3s^1 3p^1(^3P)7p^1(^2P_{3/2})$	0.0005	0.0007
1f	93.52	$3s^2 3p^1(^2P_{3/2})$-$3s^1 3p^1(^3P)7p^1(^2D_{5/2})$	0.0038	0.0041
1g	93.56	$3s^2 3p^1(^2P_{1/2})$-$3s^1 3p^1(^1P)7p^1(^2D_{3/2})$	0.0017	0.0014
1h	93.61	$3s^2 3p^1(^2P_{3/2})$-$3s^1 3p^1(^1P)7p^1(^2S_{1/2})$	0.0011	0.0010
1i	93.69	$3s^2 3p^1(^2P_{1/2})$-$3s^1 3p^1(^3P)7p^1(^4P_{3/2})$	0.0003	0.0004
Total			0.0117	0.0141

The measured Ar^{5+} ground-state ionization potential from the photoionization experiment of 91.29±0.01 eV compares with the value of 91.00 eV in the NIST database. The $^2P_{1/2}$-$^2P_{3/2}$ fine-structure splitting was determined from two independent measurements to be 0.285±0.009 eV, which compares with the NIST tabulated value of 0.274 eV. The series limits and quantum defects of several Rydberg series identified in photoionization are in reasonable agreement with the Cowan code prediction. In the energy range from 90 to 111 eV, indirect $3s$-np ($n > 6$) excitation-autoionization dominates. Shifting the photoionization spectrum calculated using the Cowan atomic structure code by +1.23 eV brings it into reasonable agreement with the resonant component of the measurement in this energy range. In the energy range from 273 to 284 eV, $2p$-$3d$ transitions are observed and the calculated photoionization spectrum is in reasonable agreement with the measurement without shifting the energy scale.

Detailed energy-scan measurements indicate that the electron-impact ionization cross section for Ar^{5+} in the electron energy range from 86 to 113 eV is dominated by unresolved $3s$-nl excitation-autoionization processes. In the electron energy range from 225 to 335 eV, contributions due to $2p$-nl excitations dominate. A feature attributed to resonant-excitation double-autoionization is identified in the electron-impact ionization experiment.
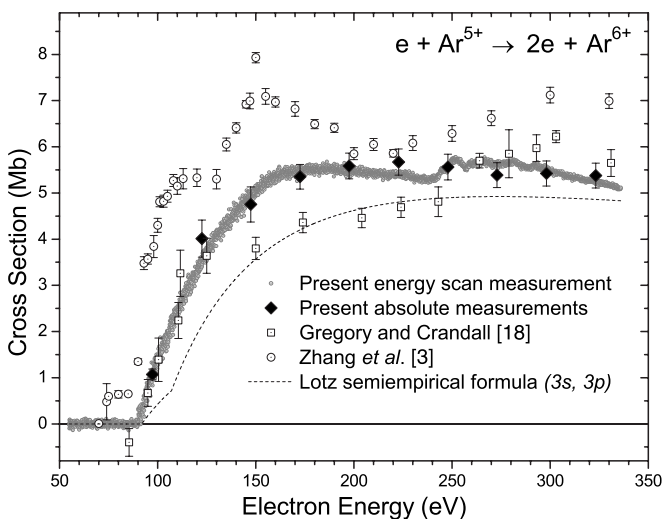
FIG. 5. Comparison of current cross-section measurements for electron-impact ionization of Ar^{5+} with previous measurements and with the Lotz semiempirical formula prediction for ionization of the $3s$ and $3p$ subshells.
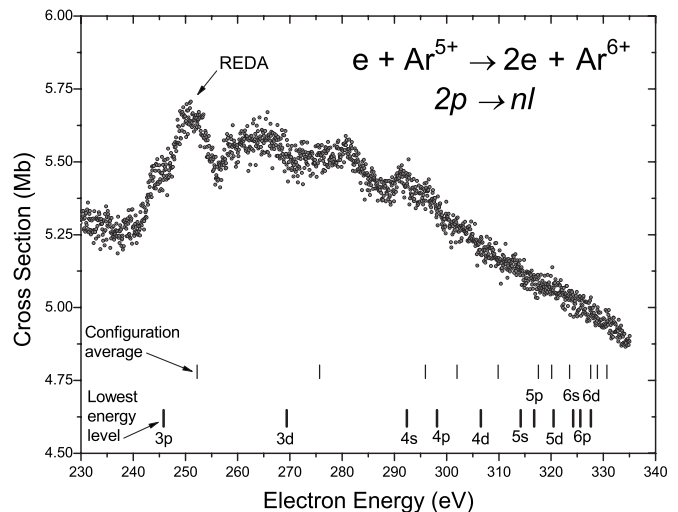

FIG. 6. Energy-scan measurement in the range from 225 to 335 eV for electron-impact ionization of Ar^{5+}. The vertical bars denote energies calculated using the Cowan code.

[1] Yu. Ralchenko, A. E. Kramida, J. Reader, W. C. Martin, A. Musgrove, E. B. Saloman, C. J. Sansonetti, and J. J. Curry, URL: http://physics.nist.gov/PhysRefData/ASD/index.html.

[2] C. Mendoza, W. Eissner, M. Le Dourneuf, and C. J. Zeippen, J. Phys. B **28**, 3485–3504 (1995).

[3] H. L. Zhang, S. Cherkani-Hassani, C. Belenger, and M. Duponchelle, J. Phys. B **35**, 3829 (2002).

[4] A. Müller, E. Salzborn, R. Frodl, R. Becker, H. Klein, and H. Winter, J. Phys. B **13**, 1877 (1980).

[5] M. J. Seaton, J. Phys. B **20**, 6363 (1987).

[6] R. Rejoub and R. A. Phaneuf, Phys. Rev. A **61**, 032706 (2000).

[7] R. Rejoub, Ph.D. thesis, University of Nevada, Reno (1998).

[8] A. M. Covington *et al.*, Phys. Rev. A **66**, 062710 (2002).

[9] A. Aguilar, Ph.D. Thesis, University of Nevada, Reno (2003).

[10] Y. Ma, C. T. Chen, G. Meigs, K. Randall, and F. Sette, Phys. Rev. A **44**, 1848 (1991).

[11] G. C. King, M. Tronc, F. H. Read, and R. C. Bradford, J. Phys. B **10**, 2479 (1977).

[12] P. Defrance, F. Brouillard, W. Claeys, and G. Van Wassenhove, J. Phys. B **14**, 103 (1981).

[13] A. Müller, K. Huber, K. Tinschert, R. Becker, and E. Salzborn, J. Phys. B **14**, 2993 (1985).

[14] A. Müller, K. Tinschert, C. Achenbach, E. Salzborn, and R. Becker, Nucl. Instrum. Methods Phys. Res. B **24**, 369 (1987).

[15] U. I. Safronova, M. Sataka, J. R. Albritton, W. R. Johnson, and M. S. Safronova, At. Data Nucl. Data Tables **84**, 1 (2003).

[16] H. Kjeldsen, P. Andersen, F. Folkmann, J. Hansen, M. Kitajima, and T. Andersen, J. Phys. B **35**, 2845 (2002).

[17] R. D. Cowan, *The Theory of Atomic Structure and Spectra* (University of California Press, Berkeley, 1981).

[18] D. C. Gregory and D. H. Crandall, Controlled Fusion Atomic Data Center, Oak Ridge National Laboratory, 1982 (unpublished), URL: http://www-cfadc.phy.ornl.gov/xbeam/ar5-6.html

[19] A. Müller, G. Hofmann, K. Tinschert, and E. Salzborn, Phys. Rev. Lett. **61**, 1352 (1988).